Supplement of Geosci. Model Dev., 19, 5857–5880, 2026
https://doi.org/10.5194/gmd-19-5857-2026-supplement

Geoscientific Model Development
Open Access
EGU

Supplement of

A food crop yield emulator for integration in the compact Earth system model OSCAR (OSCAR-crop v1.0)

Xinrui Liu et al.

Correspondence to: Xinrui Liu (liuxinrui@iiasa.ac.at)

S1. Sensitivity analysis for extreme-value regions.

To provide quantitative examples of how extreme-value response regions influence aggregated results, a sensitivity analysis for some GGCM-crop-irrigation-region combinations is conducted under SSP585 where [CO_2] varies significantly over time. In the sensitivity test, global yield responses are calculated both with and without the inclusion of individual extreme-value region, together with the ratio between them (red dashed lines in the Fig. ST1 below).

Given the large number of GGCM-crop-irrigation-region combinations, a comprehensive assessment of all extreme cases is impractical. Instead, we focus on representative cases to illustrate the potential magnitude of their influence.

As shown in the Fig. ST1, when all the extreme value regions are masked, the global aggregated CO_2-yield response follows a relatively smooth and gradual trajectory across all cases. In contrast, under higher [CO_2], including one extreme-value region can amplify the global aggregated result by up to a factor of three (e.g., CYGMA1p74-*swh*-*noirr*-JOR). Notably, both the magnitude and onset of this amplification vary across models and regions. For example, the PROMET-*ri2*-*noirr*-GMB case exhibits an abrupt transition at around 600 ppm (baseline ~400 ppm, corresponding to 2015 levels), whereas other cases show a more gradual divergence. This highlights the importance of carefully considering the input domain when interpreting results from regions with extreme response behavior.

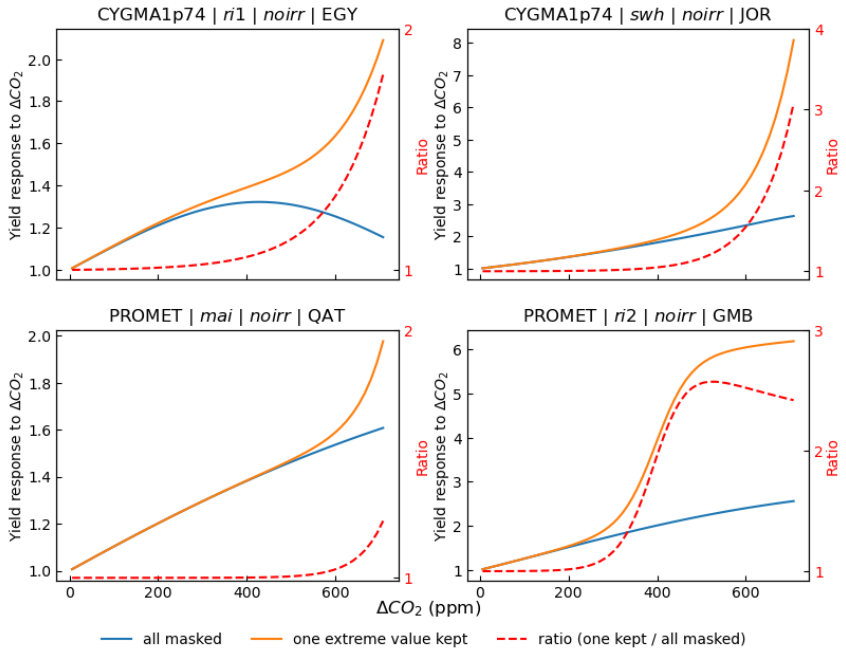

Figure S1. Global CO_2-yield response with (orange lines) and without (blue lines) the inclusion of one extreme-value region, along with their ratio (red-dashed lines; inclusion vs. exclusion). EGY, JOR, QAT, and GMB are the codes for Egypt, Jordan, Qatar, and Gambia, respectively.

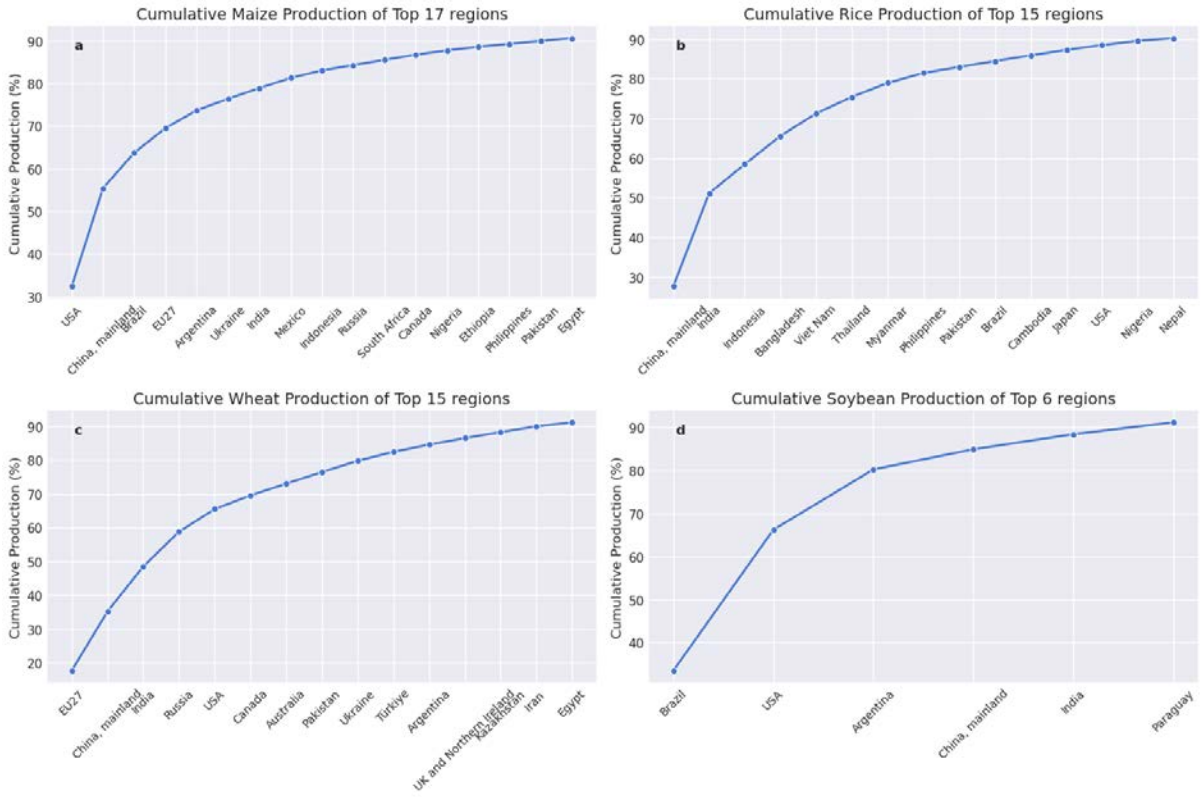

Figure S2. Top producing regions during the period of 2014 to 2023.

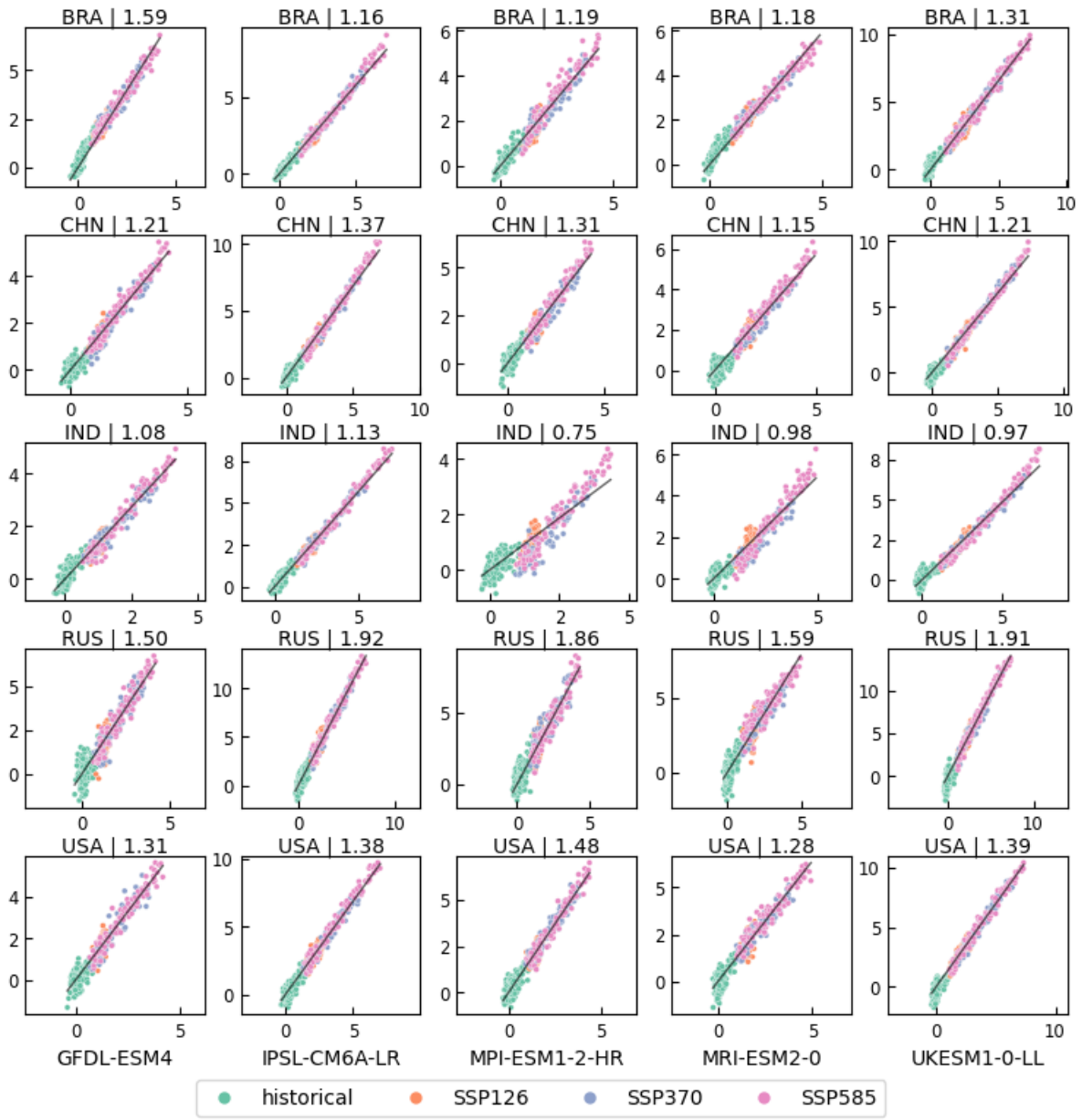

Figure S3. Relationship between global mean temperature differences and local temperature differences using the first concatenation scheme. Subplots in each row and column represent results from different countries (Brazil, China, India, Russia, and the USA) and ESMs (GFDL-ESM4, IPSL-CM6A-LR, MPI-ESM1-2-HR, MRI-ESM2-0 and UKESM1-0-LL). The values next to the regional code represent the linear coefficients.

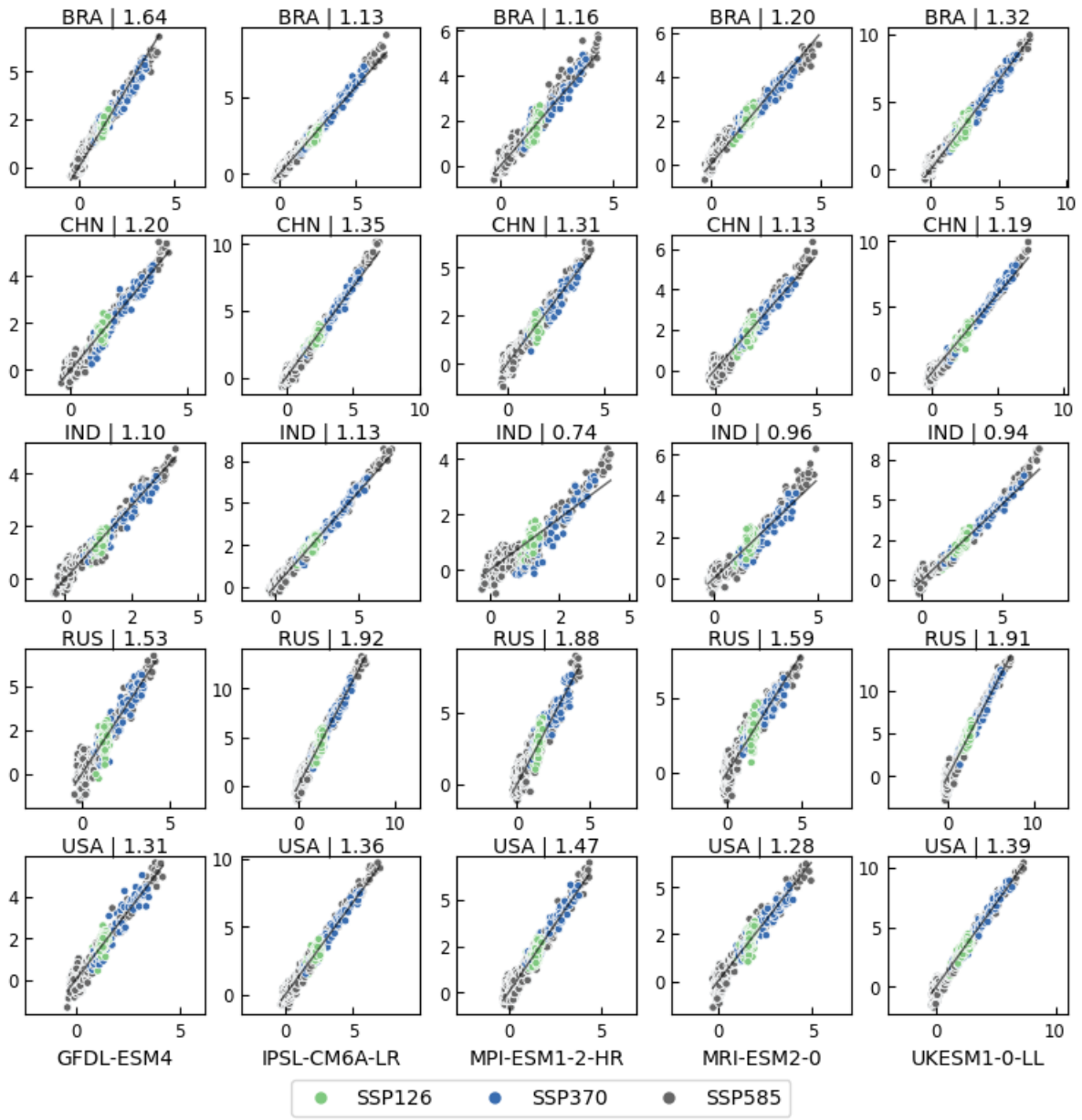

Figure S4. Relationship between global mean temperature differences and local temperature differences using the second concatenation scheme. Subplots in each row and column represent results from different countries (Brazil, China, India, Russia, and the USA) and ESMs (GFDL-ESM4, IPSL-CM6A-LR, MPI-ESM1-2-HR, MRI-ESM2-0 and UKESM1-0-LL), respectively. The values next to the regional code represent the linear coefficients.

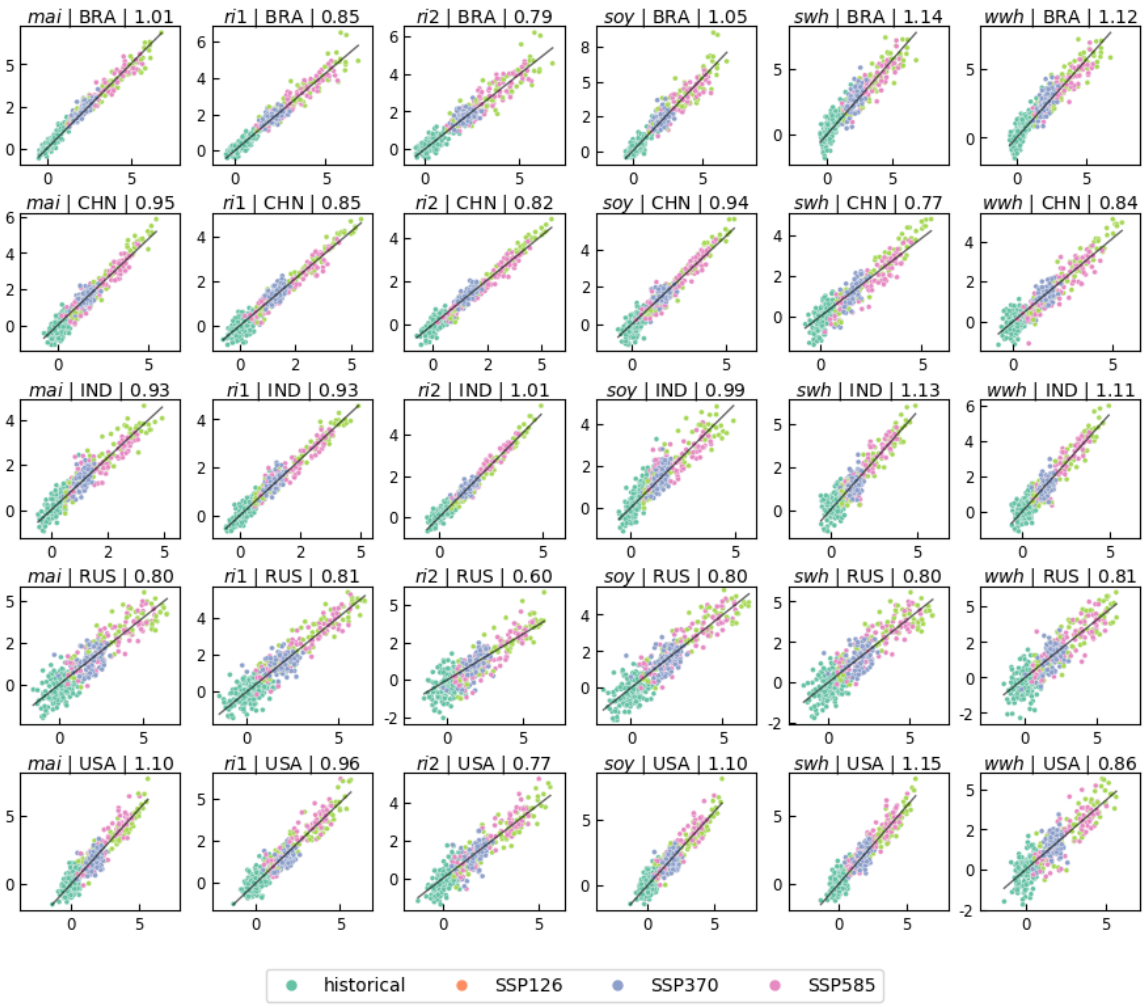

Figure S5. Relationship between local temperature differences and crop-specific growing season temperature differences under rainfed condition using the first concatenation scheme. Subplots in each row and column represent results from different countries (Brazil, China, India, Russia, and the USA) and crop species. The results are from GFDL-ESM4. The values next to the regional code represent the linear coefficients.

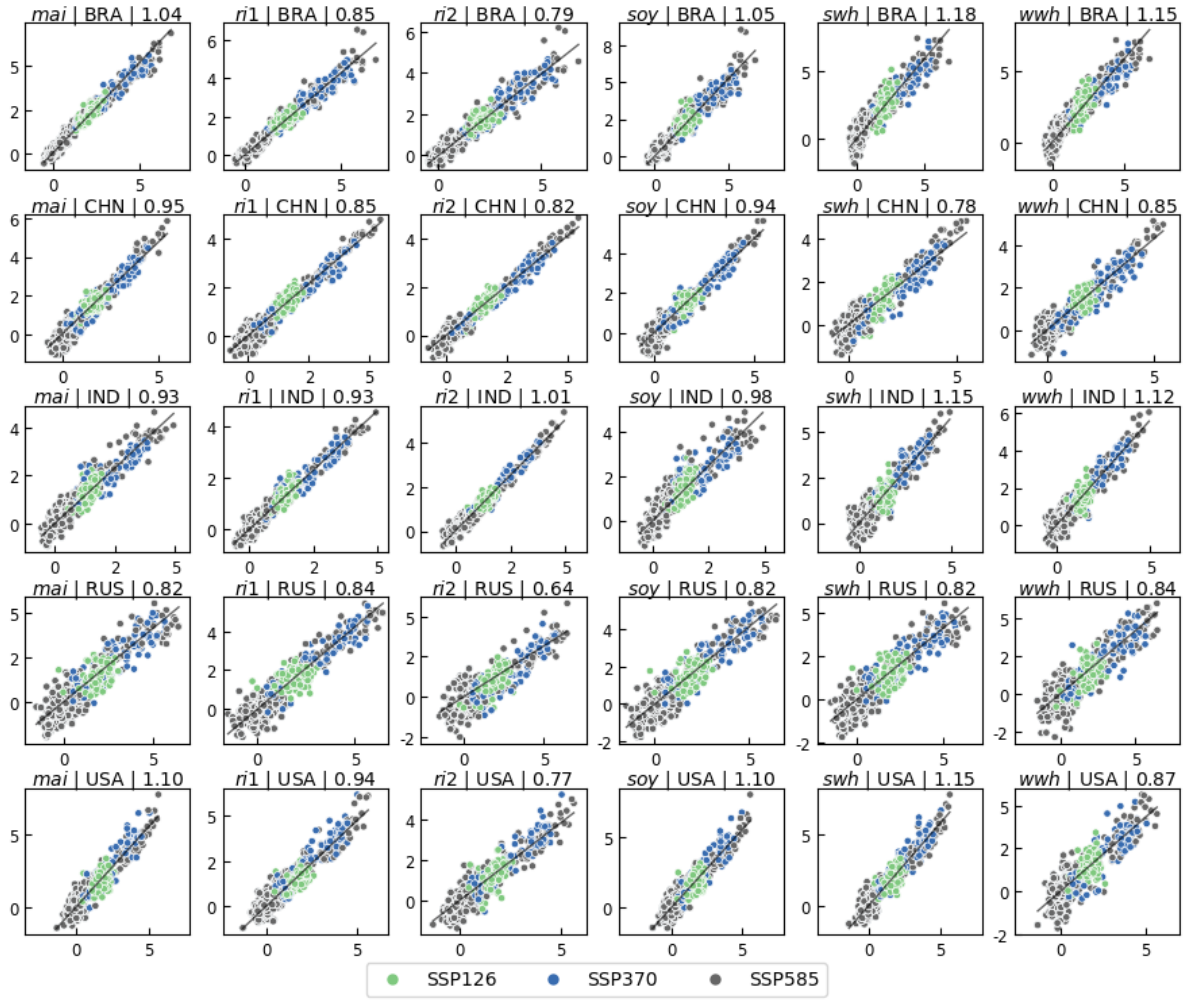

Figure S6. Relationship between local temperature differences and crop-specific growing season temperature differences under rainfed condition using the second concatenation scheme. Subplots in each row and column represent results from different countries (Brazil, mainland China, India, Russia, and the USA) and crop species. The results are from GFDL-ESM4. The values next to the regional code represent the linear coefficients.

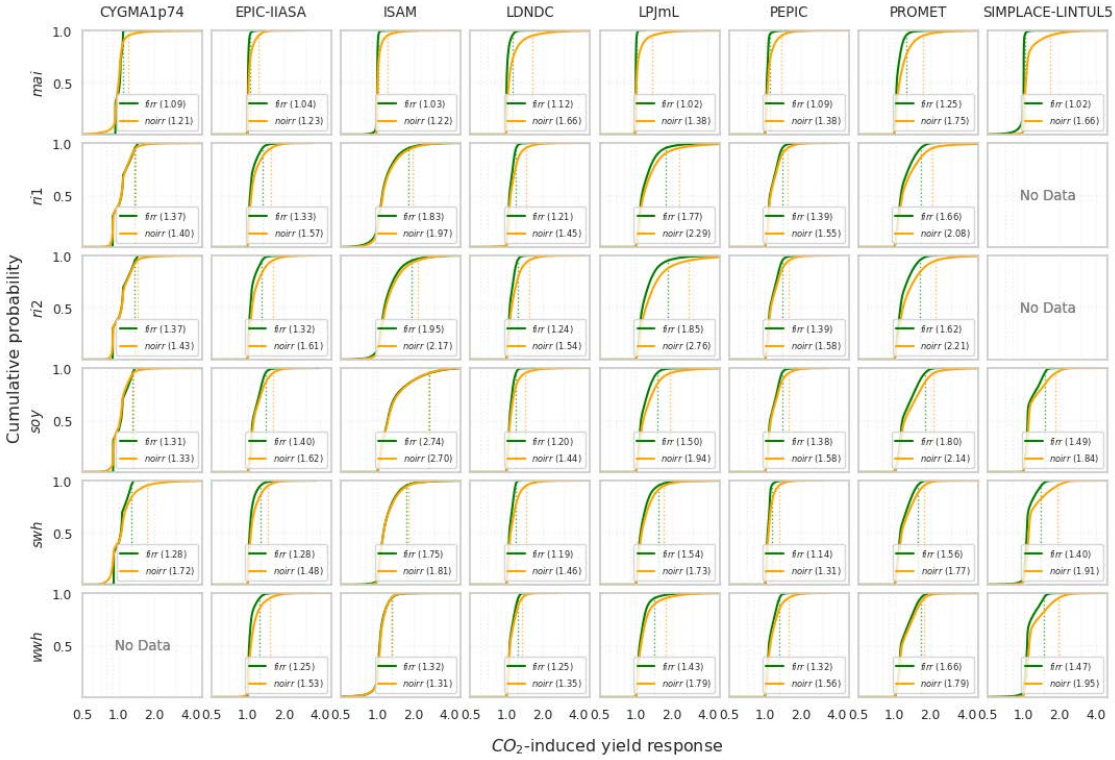

Figure S7. Cumulative probability of regional crop- and model-specific yield responses induced by CO_2. Values in the brackets represent the 95% percentiles of *firr* and *noirr* crops.

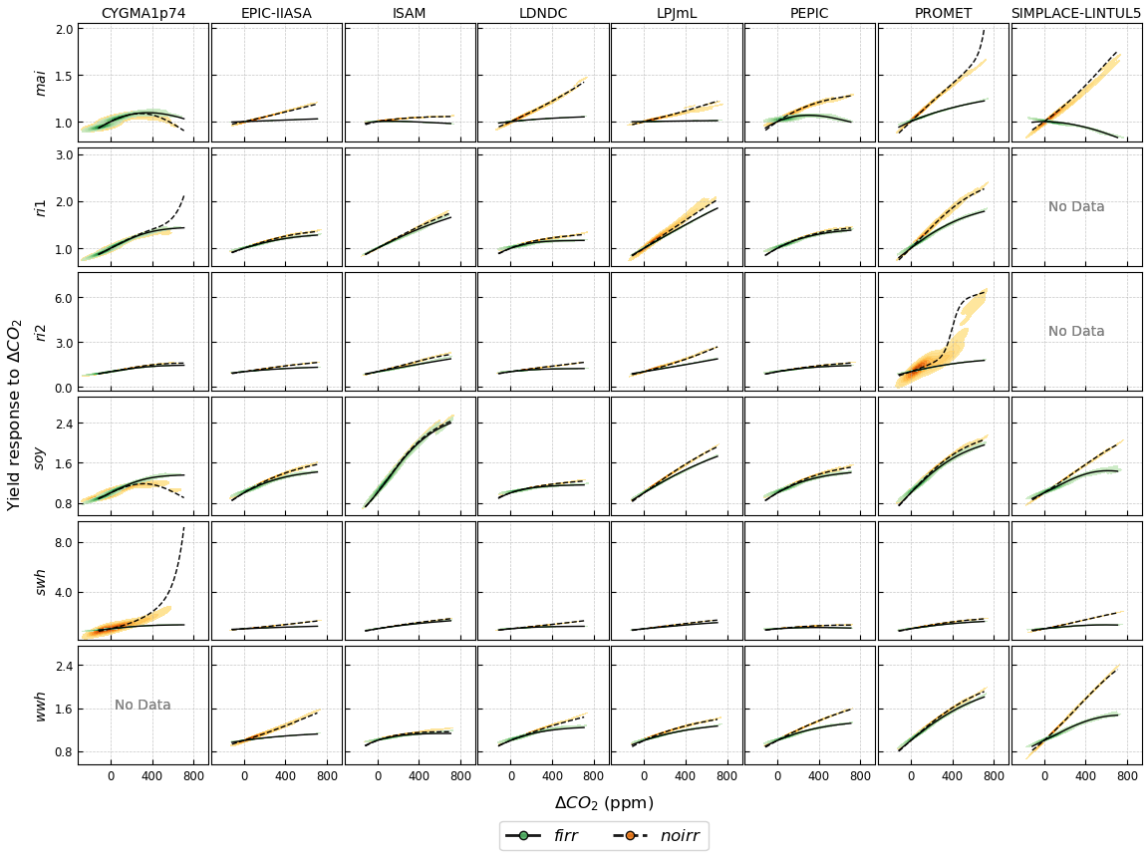

Figure S8. Kernel density estimation of global crop yield responses [CO_2] change (ppm) across eight GGCMs under historical, SSP126, SSP370, and SSP585, including extreme-value regions. Black lines indicate aggregated results from the crop emulator. Black lines indicate aggregated results from the crop emulator. Green shades and orange shades represent *firr* and *noirr* conditions, separately. Darker shades suggest higher density.

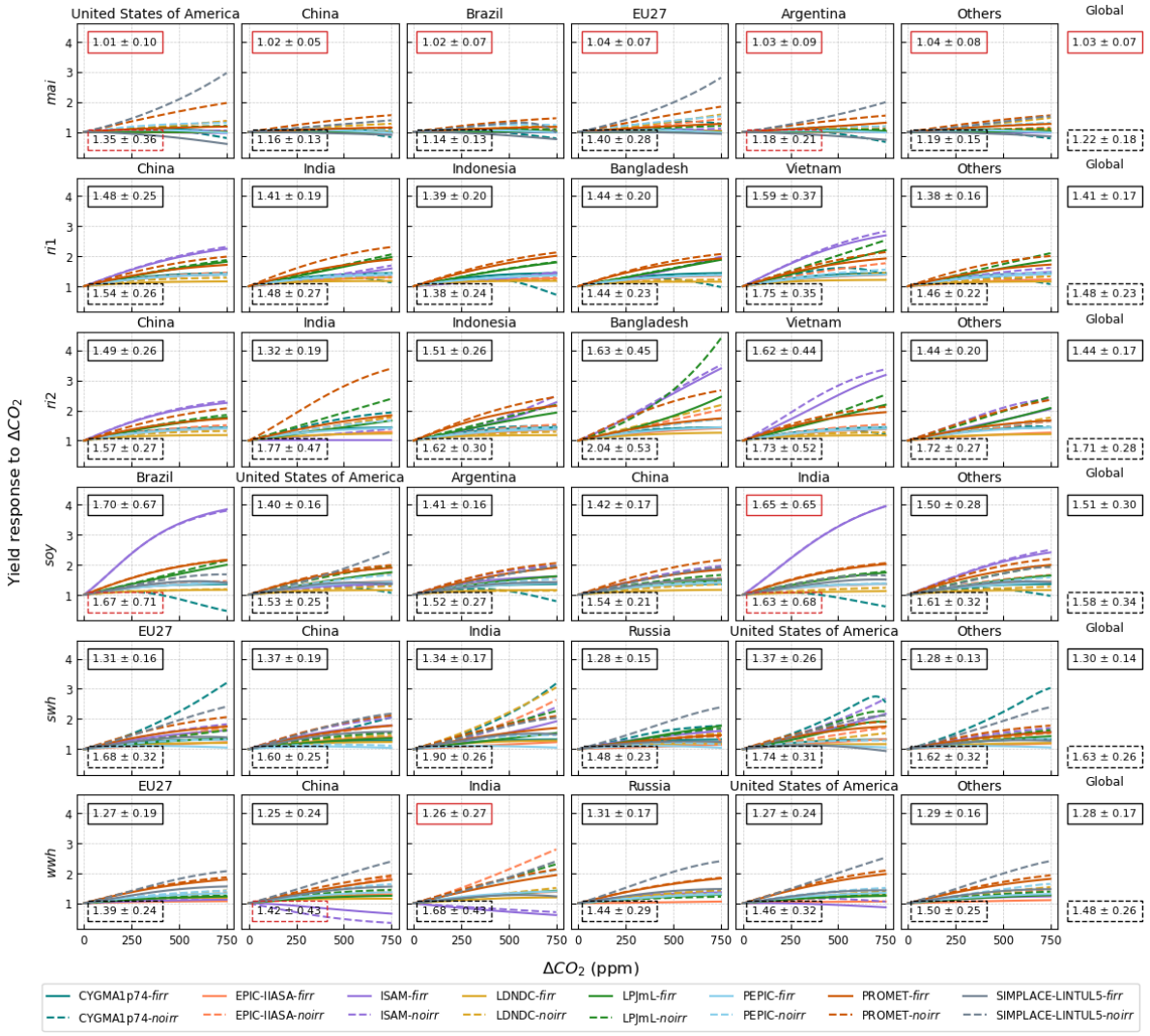

Figure S9. Region- and crop-specific yield responses to [CO_2] change (ppm). Boxes show averages and standard deviations of end-of-century (2069–2099) yield responses for *firr* (solid lines) and *noirr* (dashed lines) crops under SSP585. Red box outlines indicate negative net yield responses.

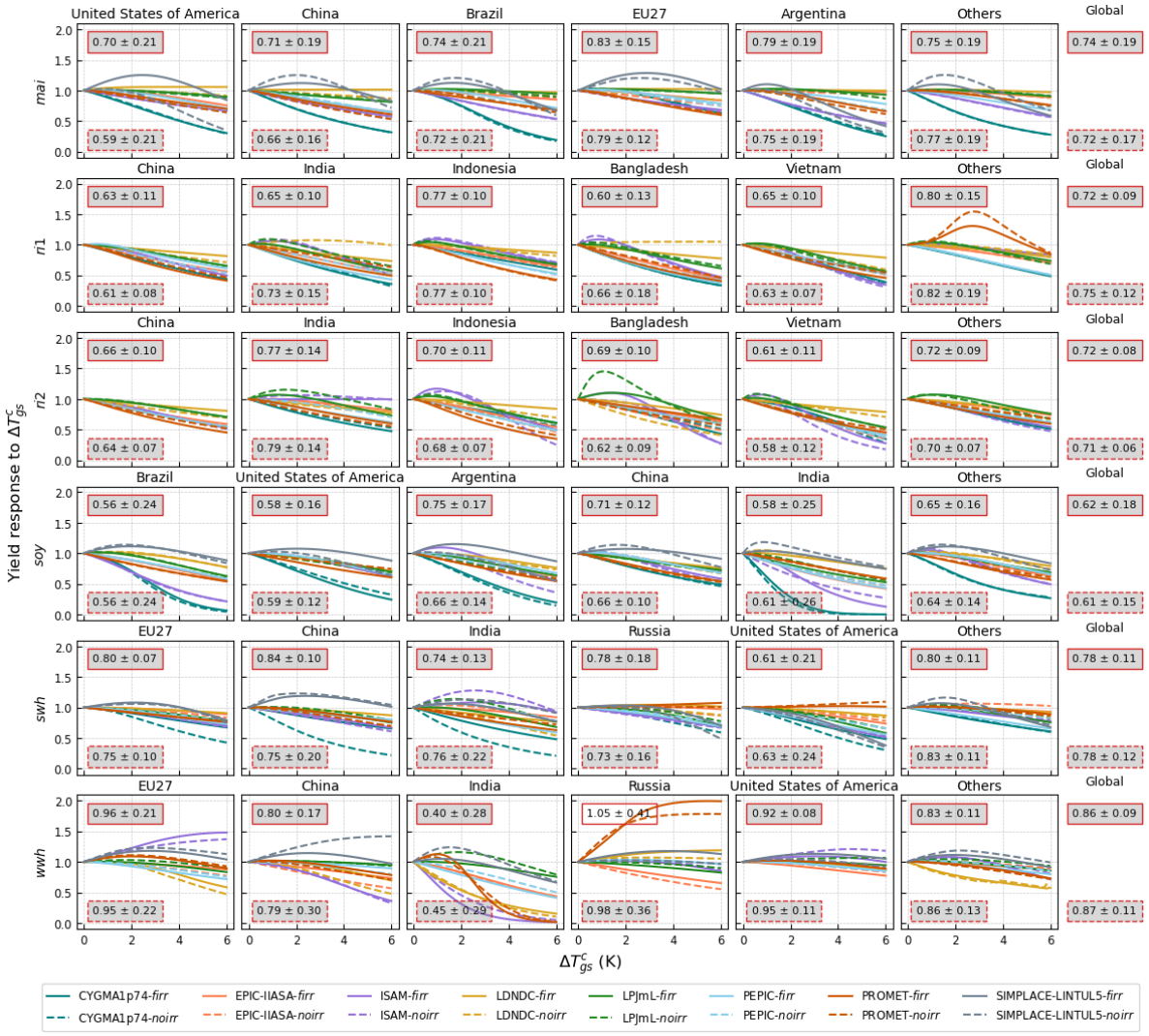

Figure S10. Region- and crop-specific yield responses to growing season temperature change (K). Boxes show averages and standard deviations of end-of-century (2069–2099) yield responses for *firr* (solid lines) and *noirr* (dashed lines) crops under SSP585. Boxes with gray shades indicate end-of-century negative net yield responses. Red box outlines indicate negative net yield responses.

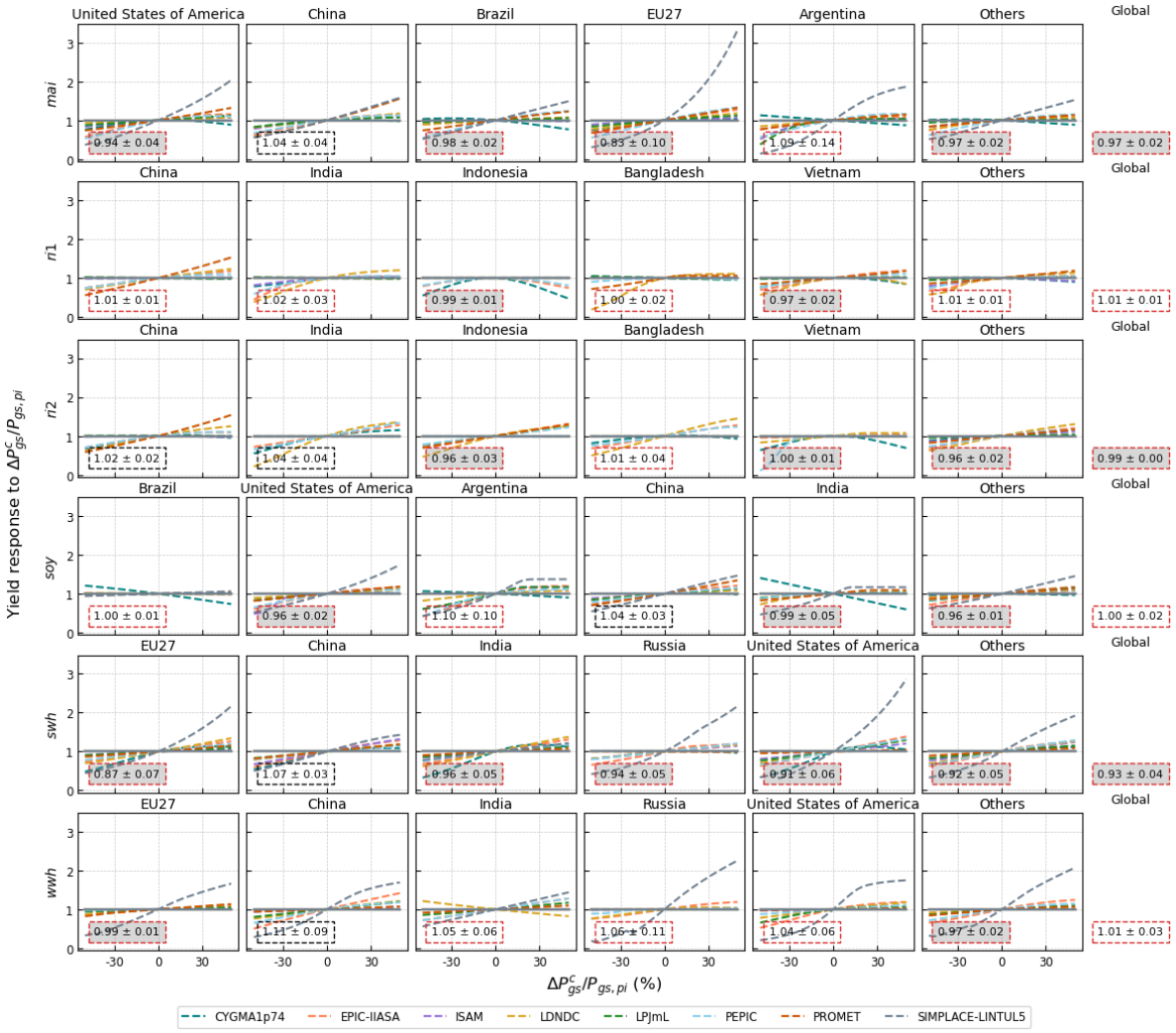

Figure S11. Region- and crop-specific yield responses to relative precipitation change (%). Boxes show averages and standard deviations of end-of-century (2069–2099) yield responses for *noirr* (dashed lines) crops under SSP585. Boxes with gray shades indicate end-of-century negative yield responses. Red box outlines indicate negative net yield responses.

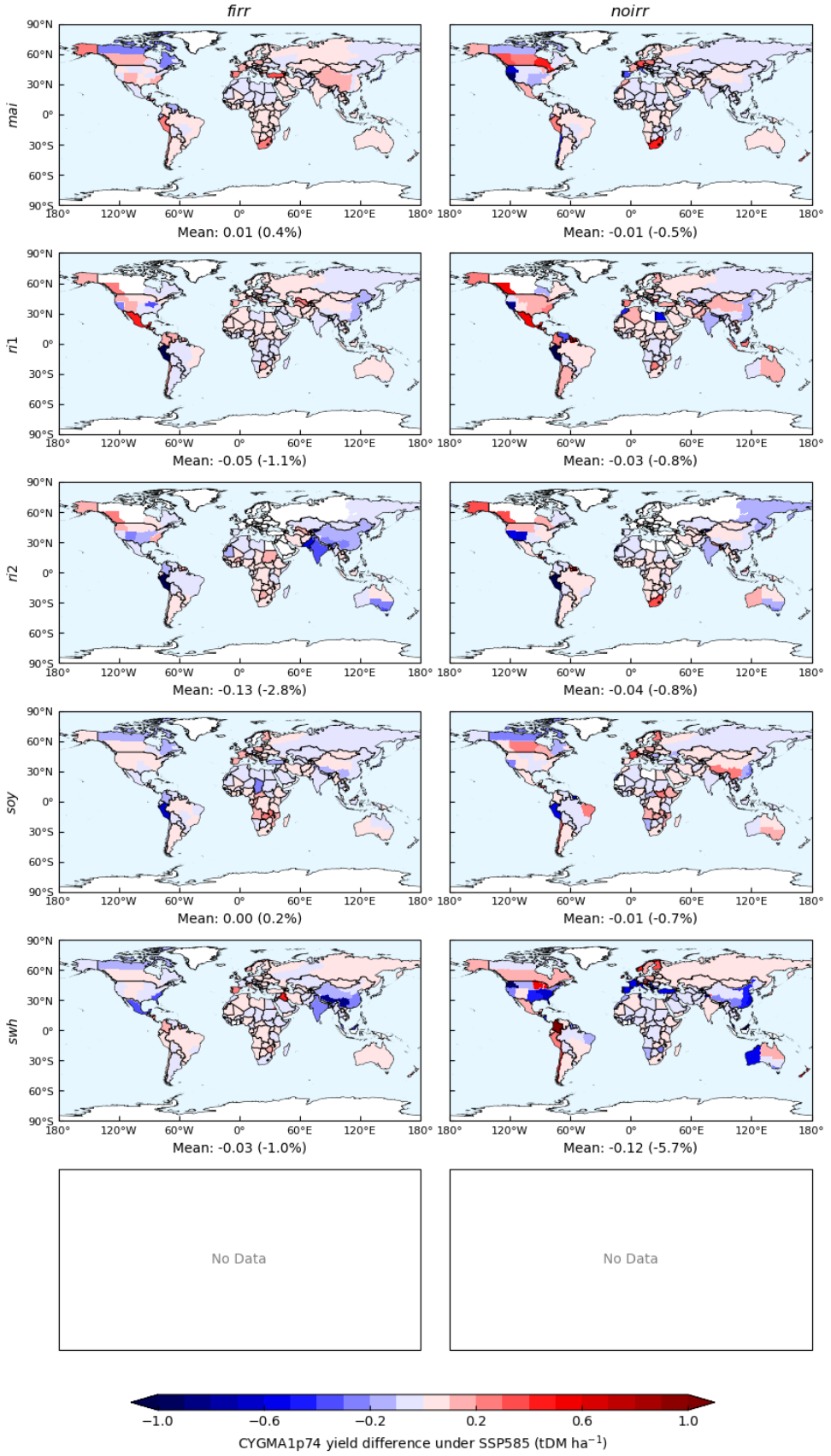

Figure S12. End-of-century yield differences between original and CYGMA1p74-based emulated crop yields under SSP585. Values below each map show the absolute and relative (in parentheses) global mean yield differences.

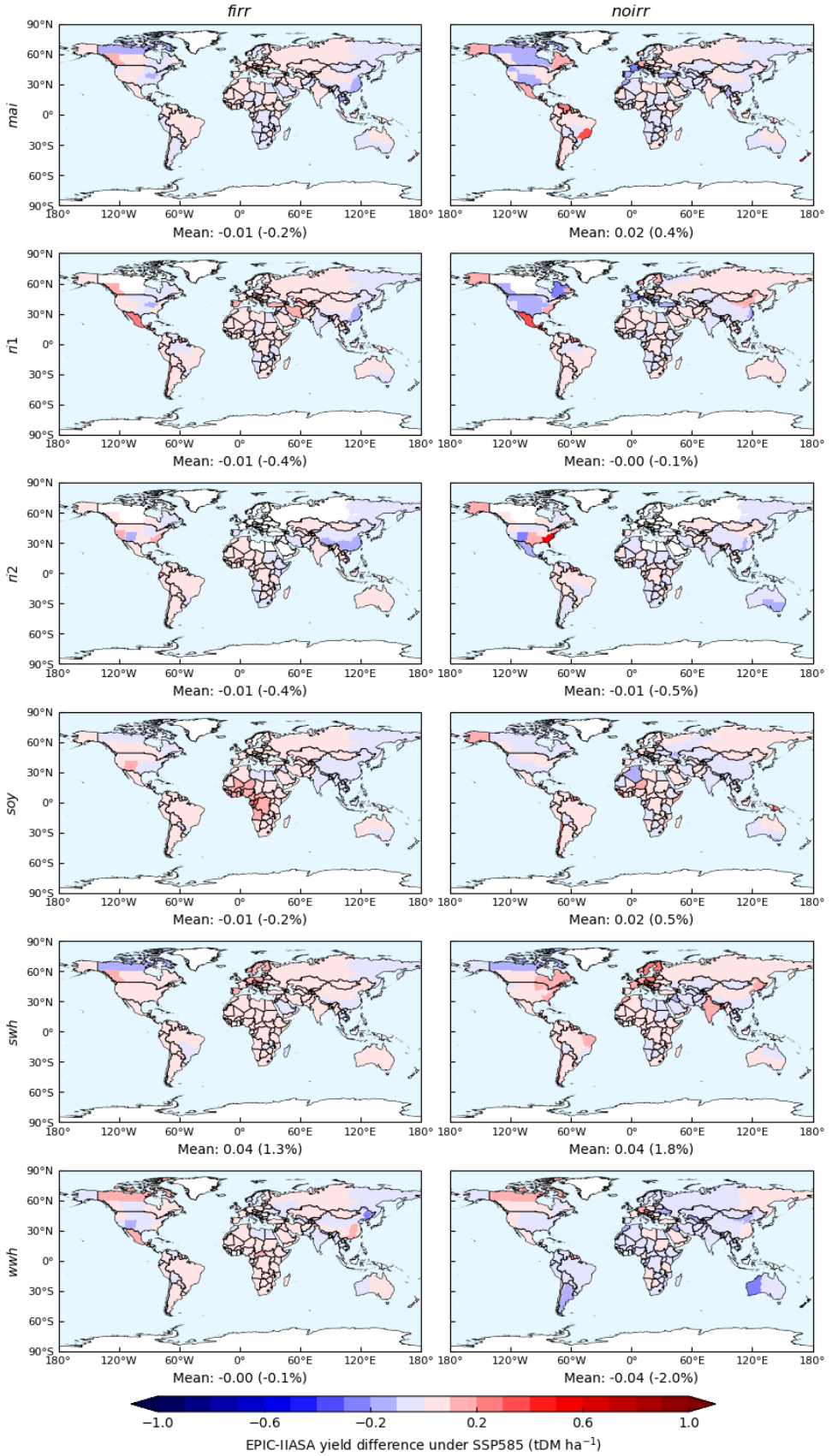

Figure S13. End-of-century yield differences between original and EPIC-IIASA-based emulated crop yields under SSP585. Values below each map show the absolute and relative (in parentheses) global mean yield differences.

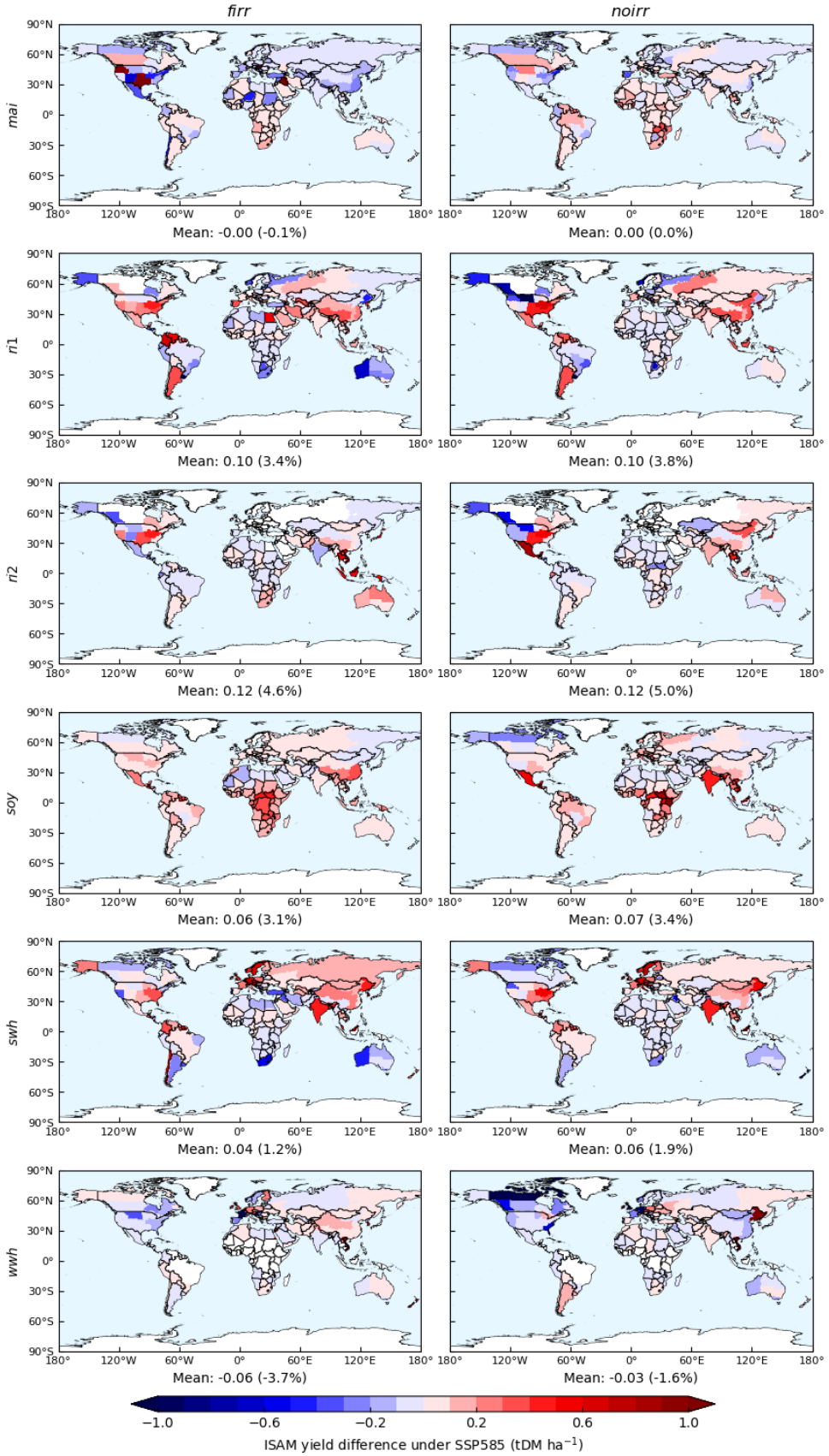

Figure S14. End-of-century yield differences between original and ISAM-based emulated crop yields under SSP585. Values below each map show the absolute and relative (in parentheses) global mean yield differences.

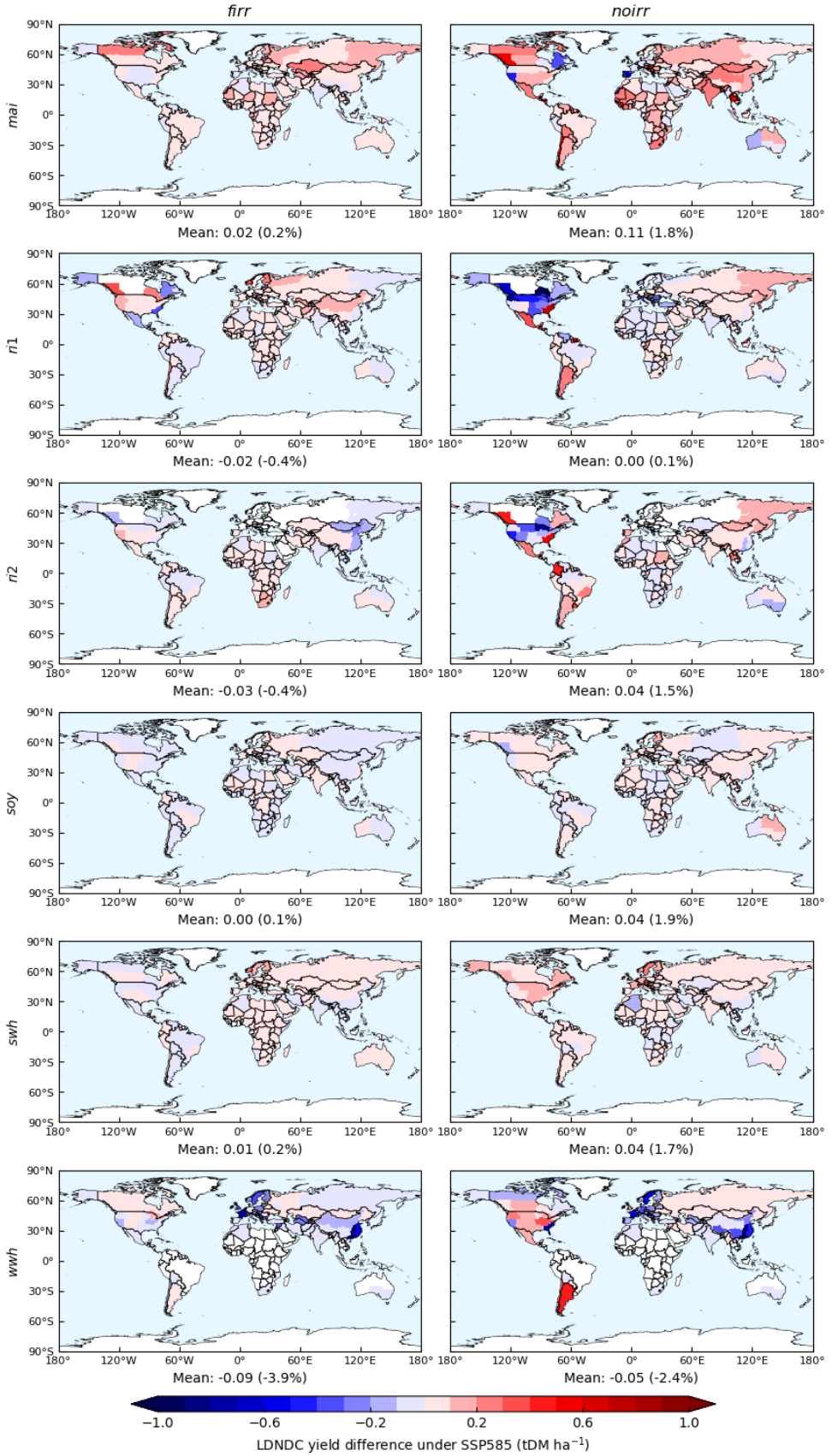

Figure S15. End-of-century yield differences between original and LDNDC-based emulated crop yields under SSP585. Values below each map show the absolute and relative (in parentheses) global mean yield differences.

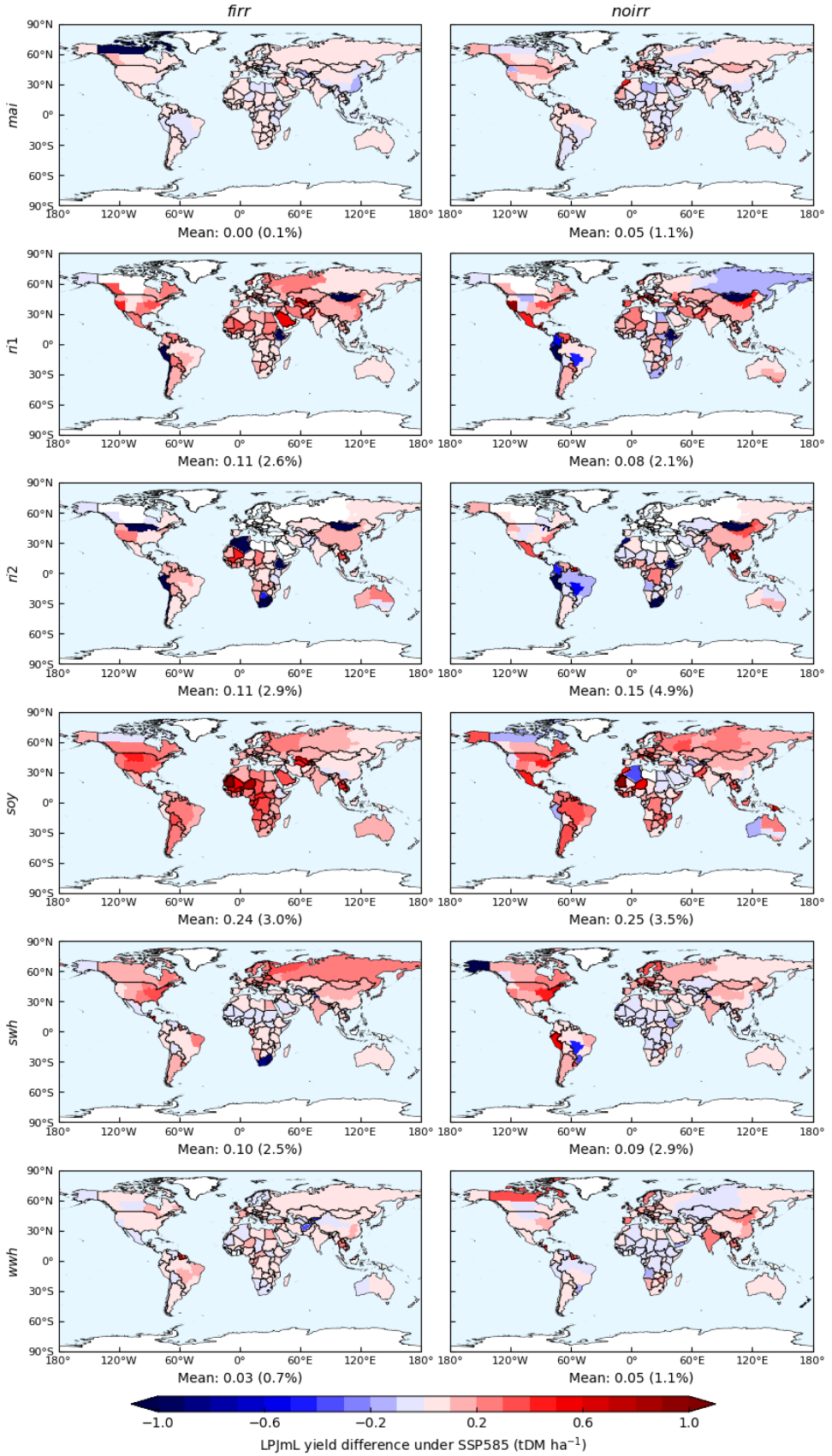

Figure S16. End-of-century yield differences between original and LPJmL-based emulated crop yields under SSP585. Values below each map show the absolute and relative (in parentheses) global mean yield differences.

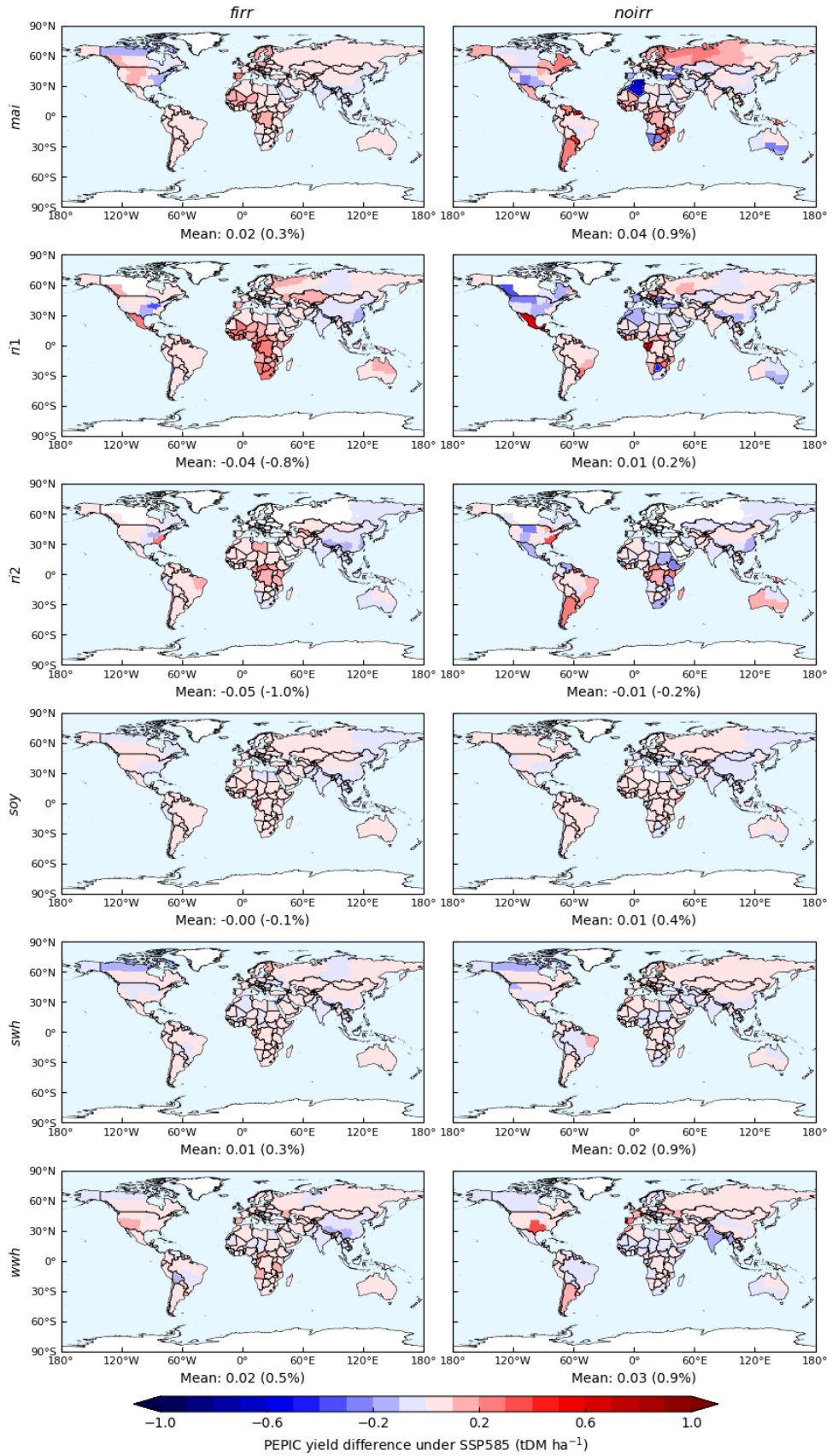

Figure S17. End-of-century yield differences between original and PEPIC-based emulated crop yields under SSP585. Values below each map show the absolute and relative (in parentheses) global mean yield differences.

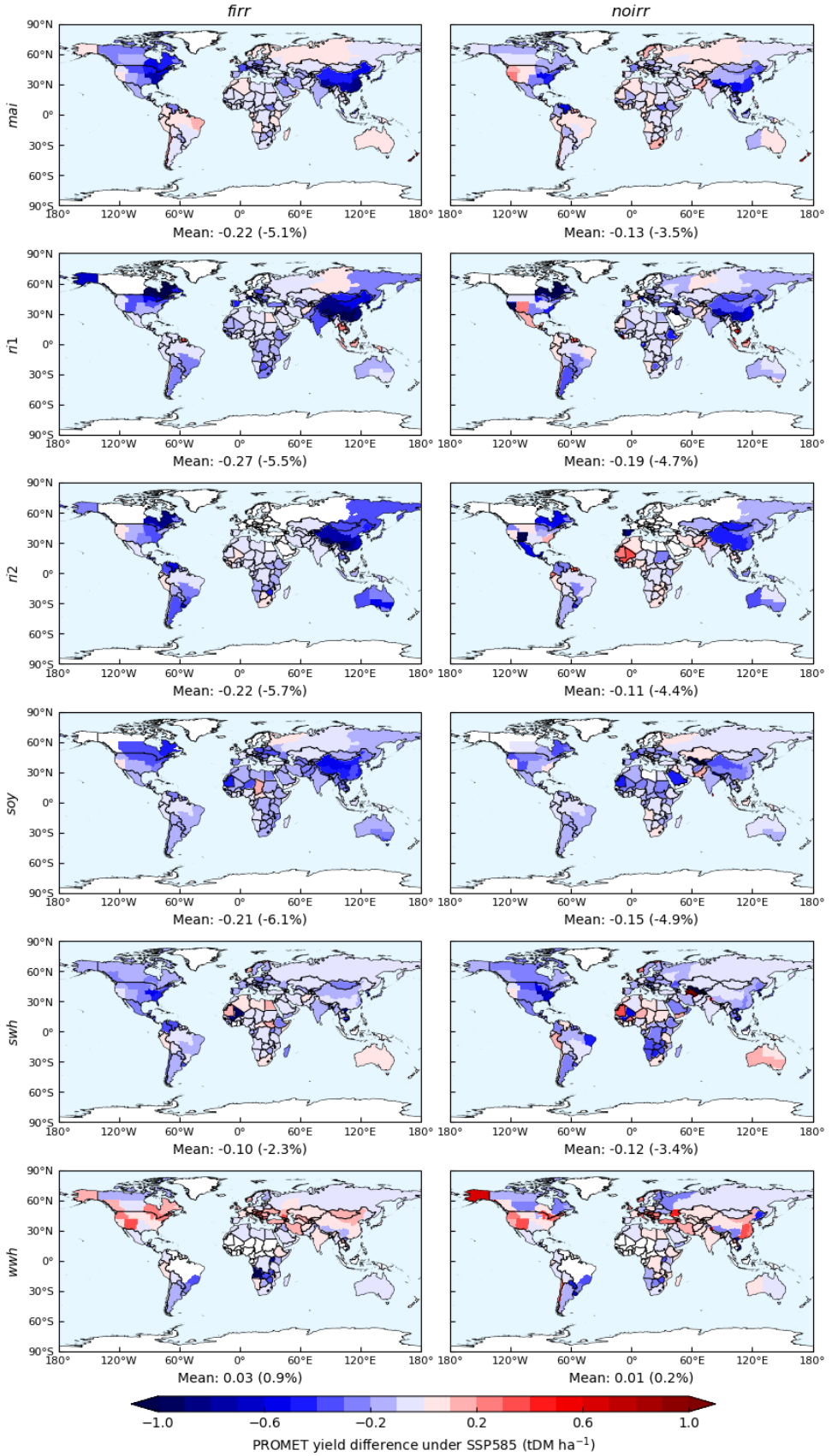

Figure S18. End-of-century yield differences between original and PROMET-based emulated crop yields under SSP585. Values below each map show the absolute and relative (in parentheses) global mean yield differences.

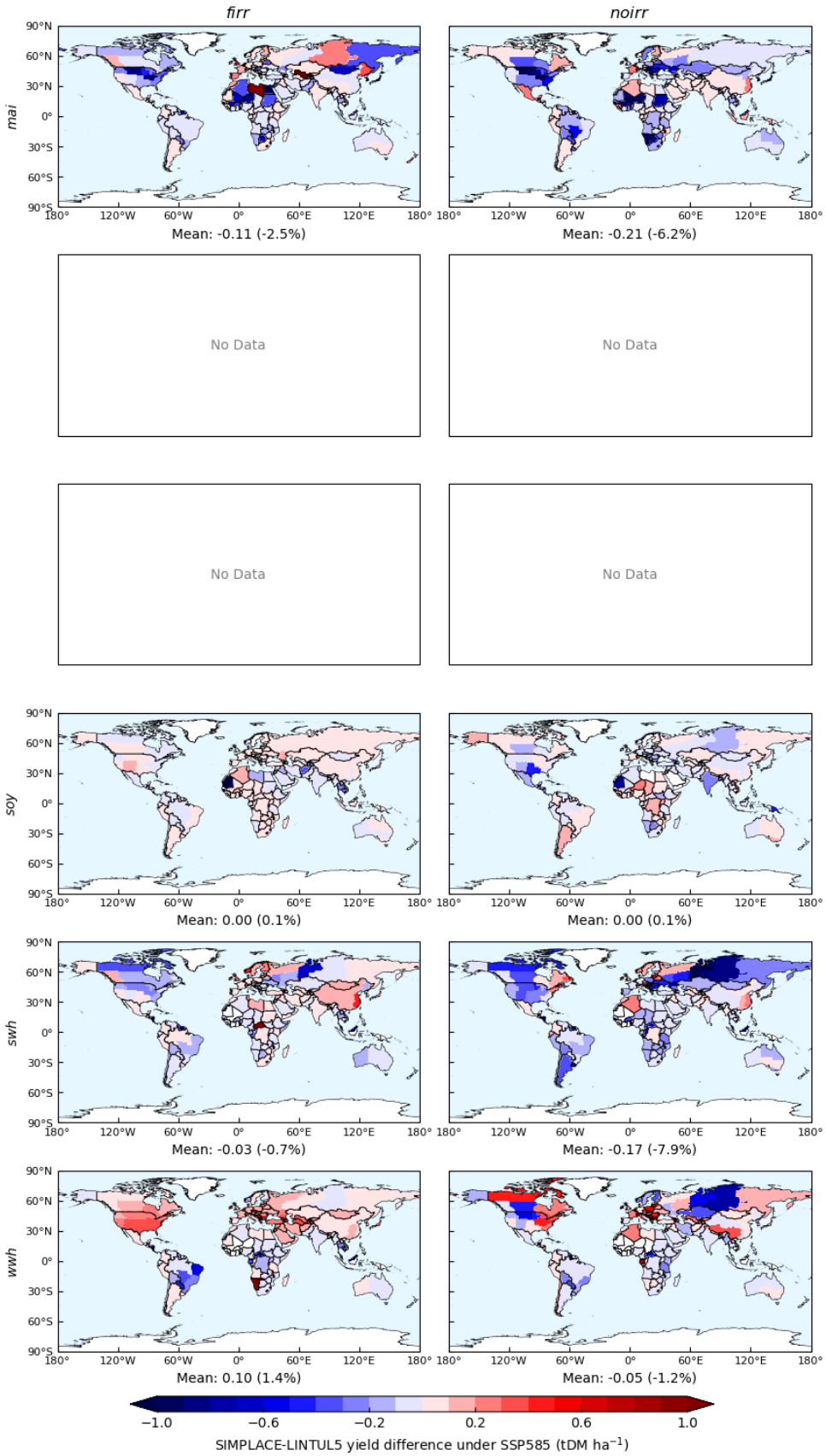

Figure S19. End-of-century yield differences between original and SIMPLACE-LINTUL5-based emulated crop yields under SSP585. Values below each map show the absolute and relative (in parentheses) global mean yield differences.

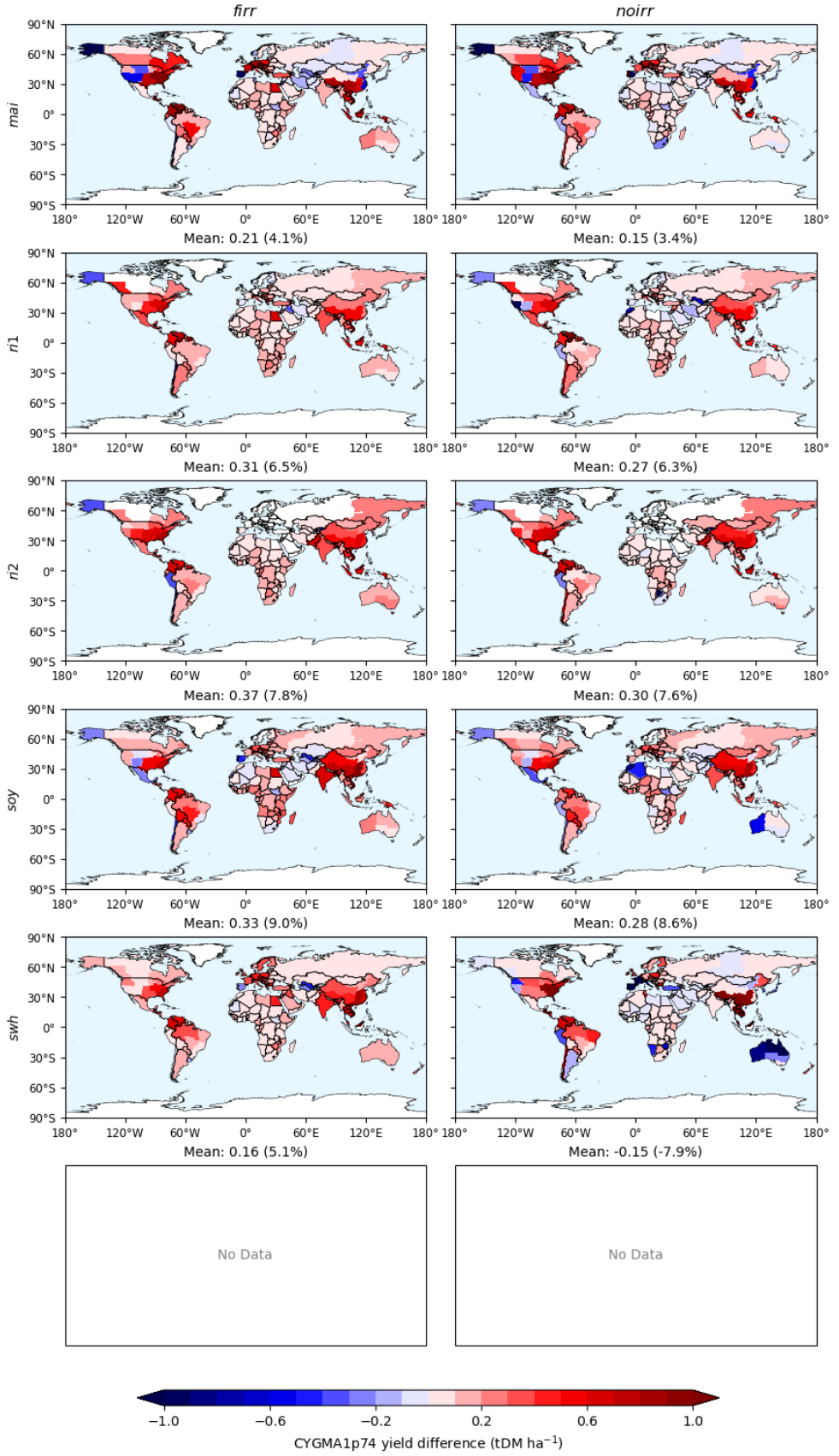

Figure S20. Yield differences between original and CYGMA1p74-based emulated crop yields under GSWP3-W5E5 climate. Values below each map show the absolute and relative (in parentheses) global mean yield differences.

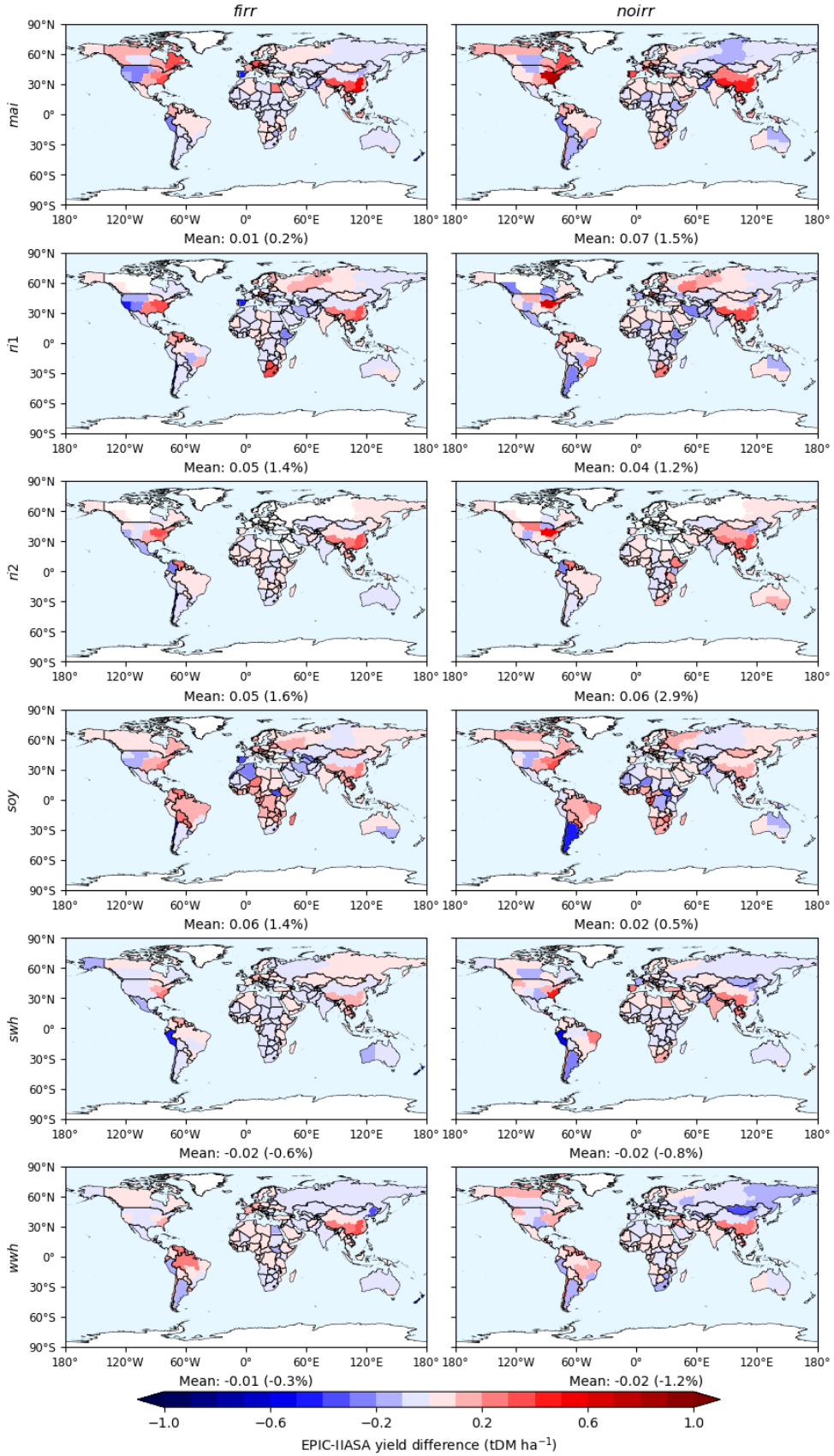

Figure S21. Yield differences between original and EPIC-IIASA-based emulated crop yields under GSWP3-W5E5 climate. Values below each map show the absolute and relative (in parentheses) global mean yield differences.

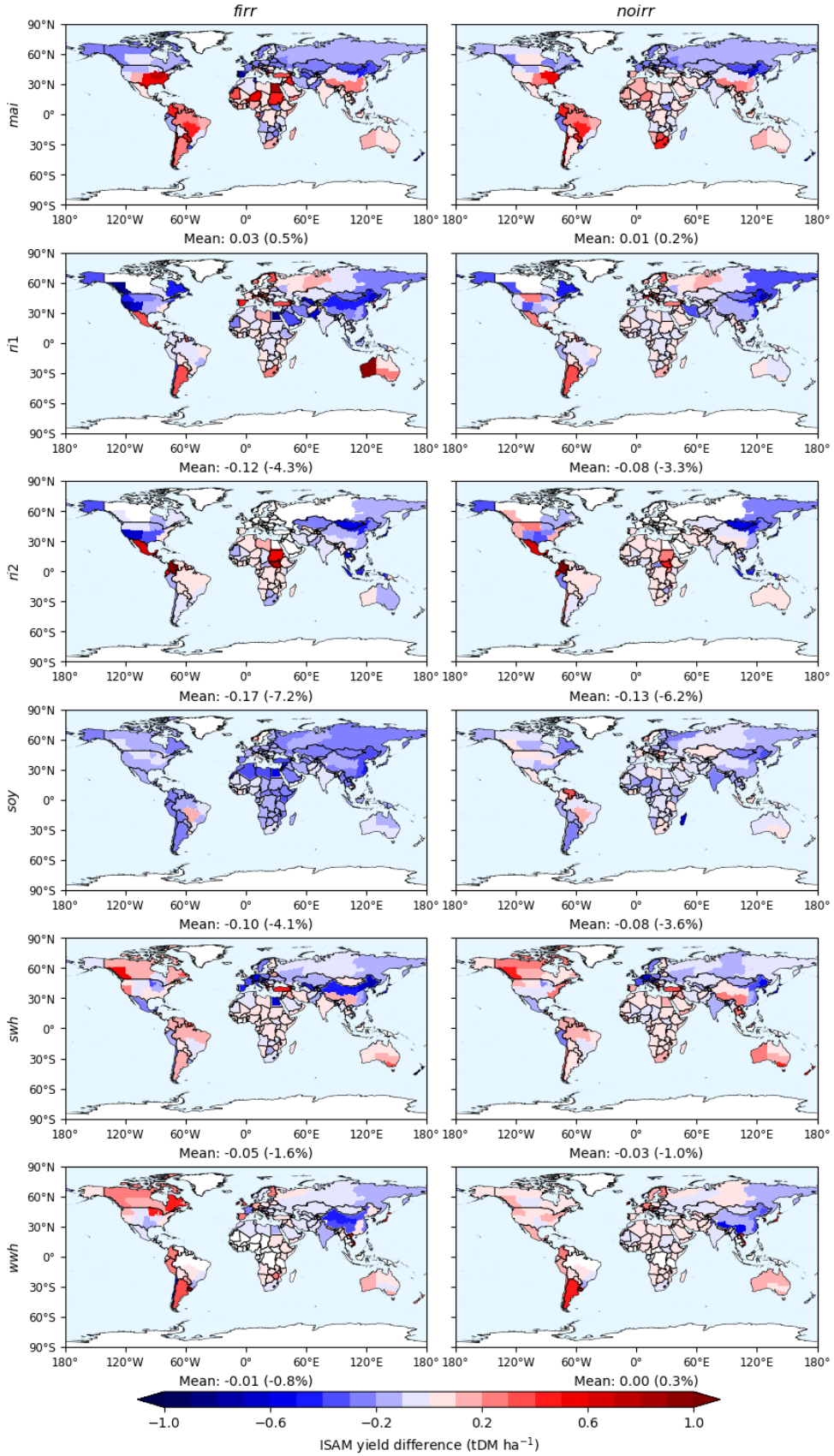

Figure S22. Yield differences between original and ISAM-based emulated crop yields under GSWP3-W5E5 climate. Values below each map show the absolute and relative (in parentheses) global mean yield differences.

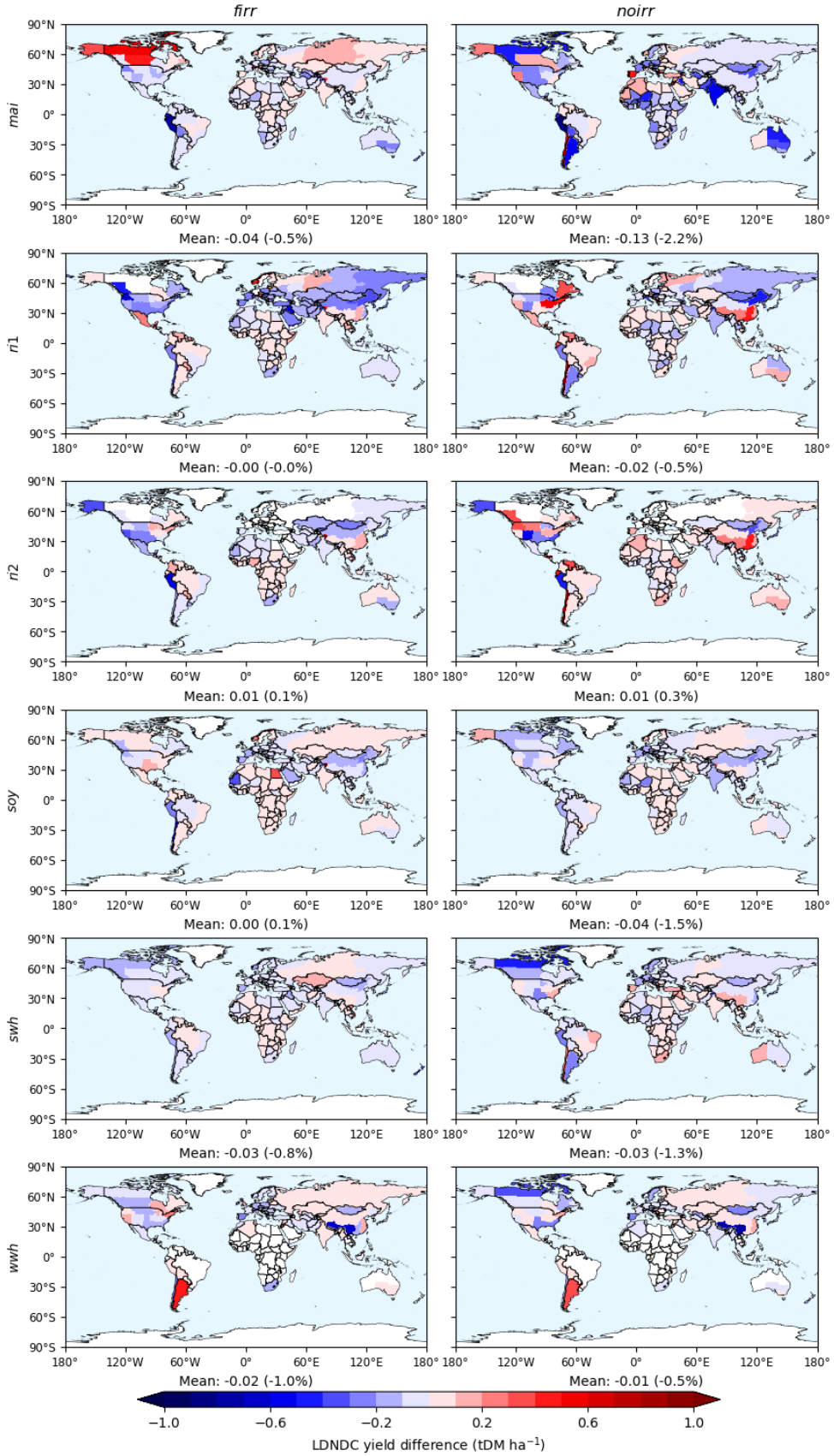

Figure S23. Yield differences between original and LDNDC-based emulated crop yields under GSWP3-W5E5 climate. Values below each map show the absolute and relative (in parentheses) global mean yield differences.

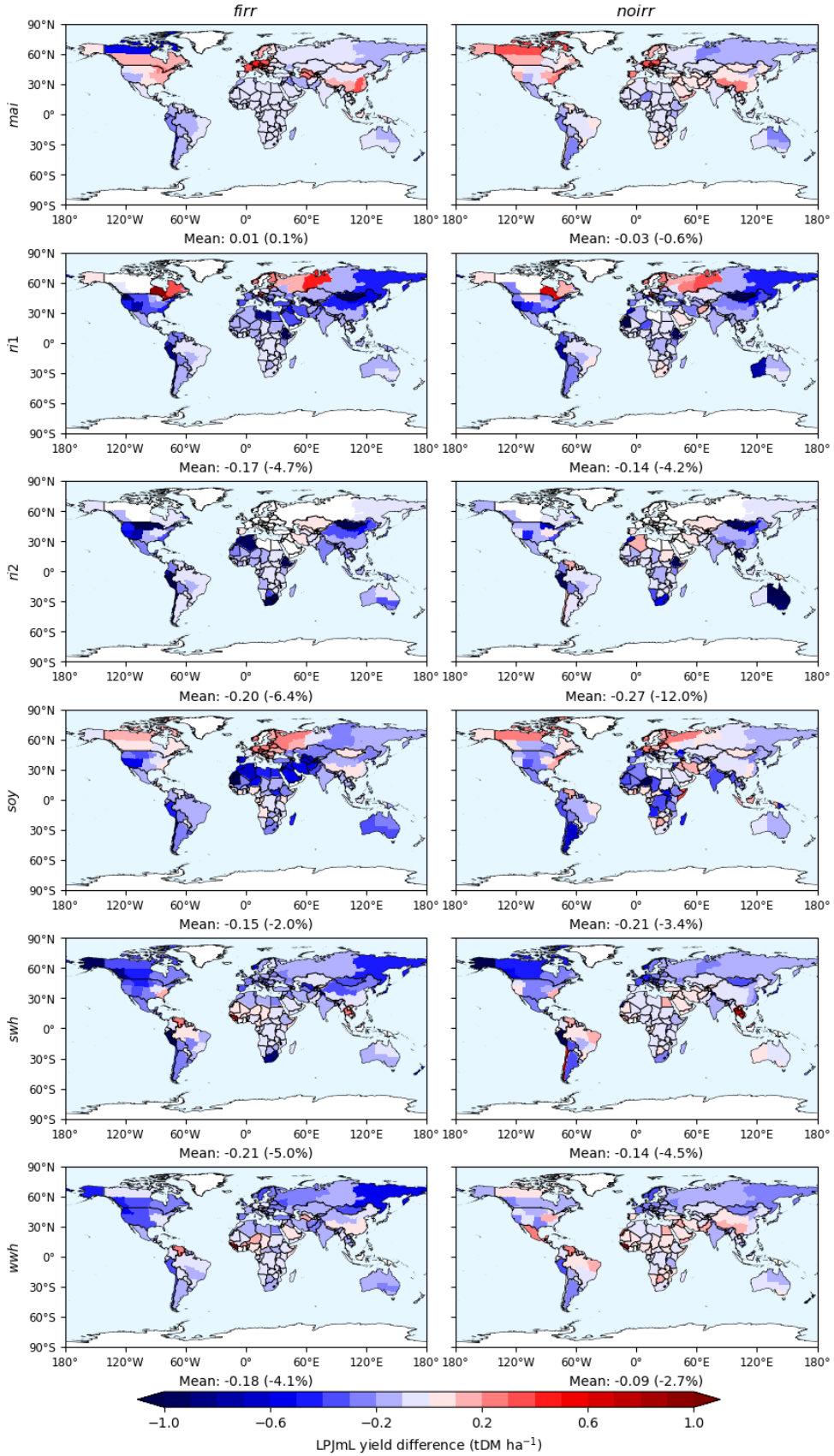

Figure S24. Yield differences between original and LPJmL-based emulated crop yields under GSWP3-W5E5 climate. Values below each map show the absolute and relative (in parentheses) global mean yield differences.

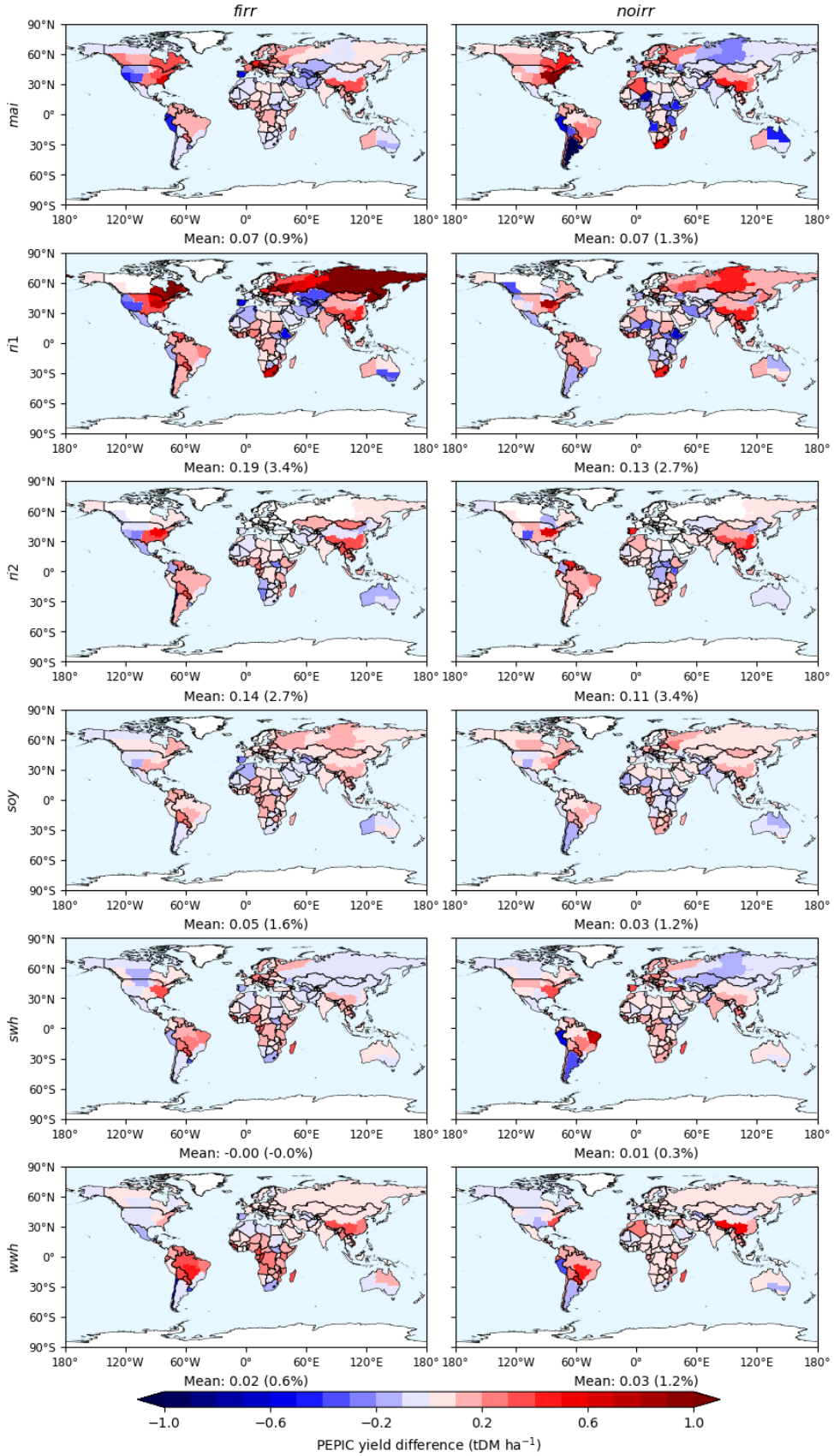

Figure S25. Yield differences between original and PEPIC-based emulated crop yields under GSWP3-W5E5 climate. Values below each map show the absolute and relative (in parentheses) global mean yield differences.

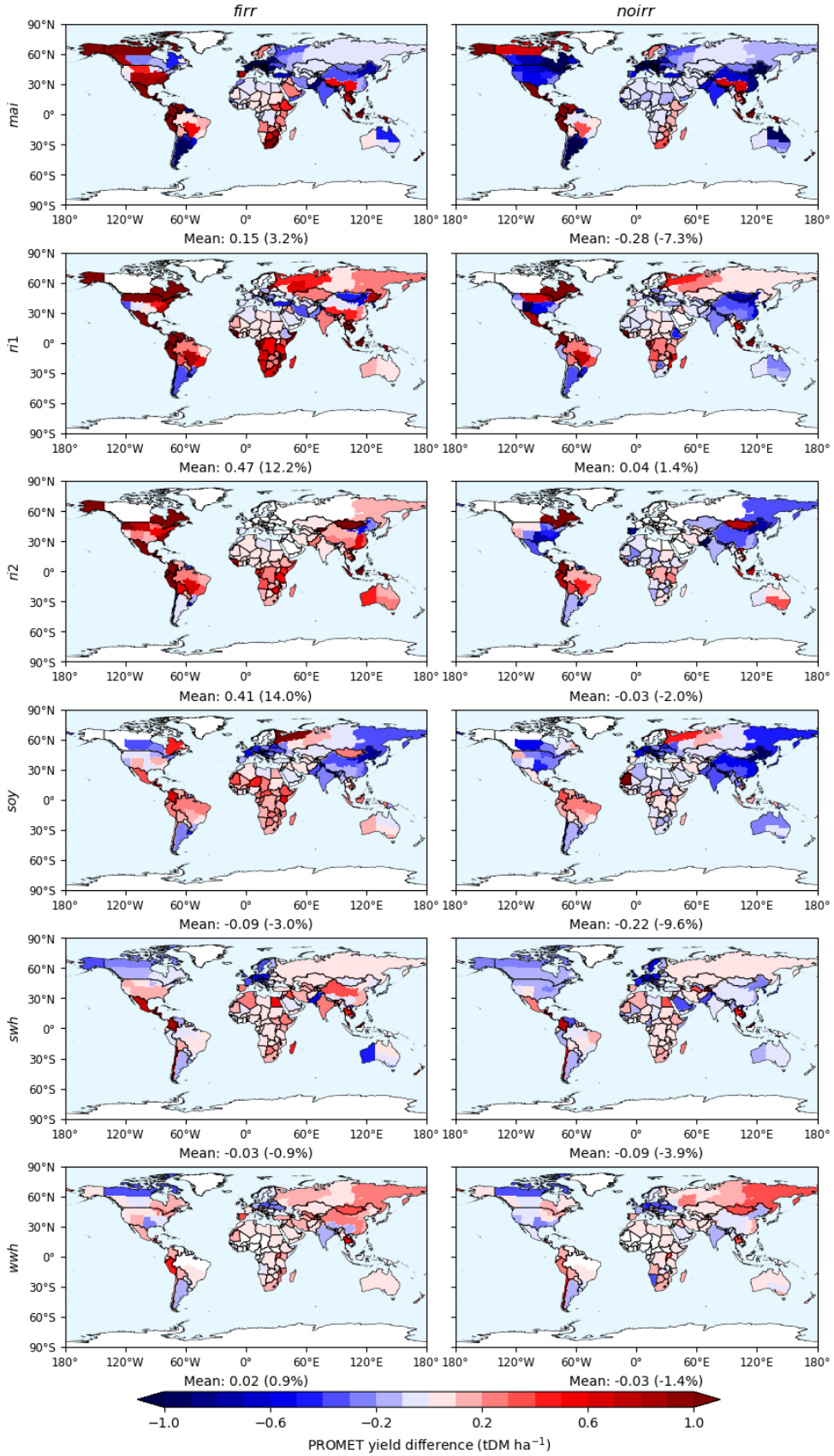

Figure S26. Yield differences between original and PROMET-based emulated crop yields under GSWP3-W5E5 climate. Values below each map show the absolute and relative (in parentheses) global mean yield differences.

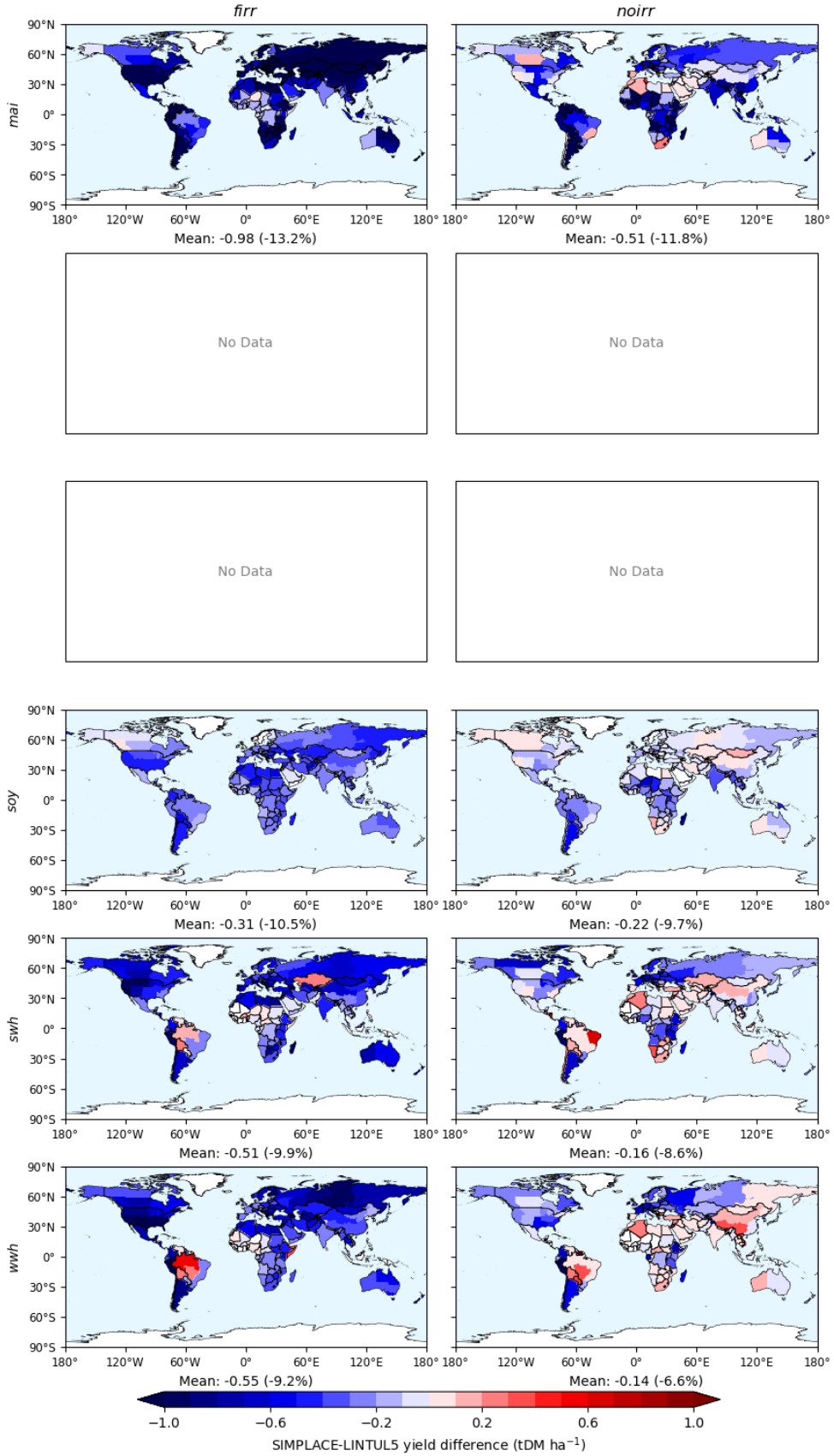

Figure S27. Yield differences between original and SIMPLACE-LINTUL5-based emulated crop yields under GSWP3-W5E5 climate. Values below each map show the absolute and relative (in parentheses) global mean yield differences.

Table S1. Six major production regions by crop.

Crop	Regions					
	R1	**R2**	**R3**	**R4**	**R5**	**R6**
Maize	USA	China	Brazil	EU27	Argentina	Others
Rice	China	India	Indonesia	Bangladesh	Vietnam	Others
Soybean	Brazil	USA	Argentina	China	India	Others
Wheat	EU27	China	India	Russia	USA	Others

Table S2. Crops and corresponding land-use categories.

Crop	Specifier	Land-use variables
Maize	*mai*	maize_rainfed, maize_irrigated
Rice (first growing season)	*ri1*	rice_rainfed, rice_irrigated
Rice (second growing season)	*ri2*	rice_rainfed, rice_irrigated
Soybean	*soy*	oil_crops_soybean_rainfed, oil_crops_soybean_irrigated
Spring wheat	*swh*	temperate_cereals_rainfed, temperate_cereals_irrigated
Winter wheat	*wwh*	temperate_cereals_rainfed, temperate_cereals_irrigated

Table S3. Functional forms and parameters for GGCM-based calibration.

Number	Functional form	Parameters	Descriptions	Maximum point	Asymptotic maximum value
①	$\alpha x + 1$	α	Linear	/	/
②	$e^{\alpha x}$	α	Exponential	/	/
③	$e^{(-\alpha \times (x-\beta)^2 + \alpha\beta^2)}$	α, β	Bell-shaped	$x = \beta$ $y = e^{\alpha\beta^2}$	/
④	$\frac{2}{e^{\alpha x} + e^{-bx}}$	α, β	Peak-and-decline	$x = \frac{ln\beta - ln\alpha}{\alpha + \beta}$ $y = \frac{2\alpha}{\alpha + \beta}(\frac{\beta}{\alpha})^{\frac{\beta}{\alpha+\beta}}$	/
⑤	$\frac{e^{\beta} + 1}{e^{-\alpha x + \beta} + 1}$	α, β	S-shaped		$y = e^{\beta} + 1$
⑥	$\frac{e^{-\alpha\gamma} + e^{\beta\gamma}}{e^{\alpha(x-\gamma)} + e^{-\beta(x-\gamma)}}$	α, β, γ	Skewed bell-shaped	$x = \gamma + \frac{ln\beta - ln\alpha}{\alpha + \beta}$ $y = \frac{\alpha(e^{-\alpha\gamma} + e^{\beta\gamma})}{\alpha + \beta}(\frac{\beta}{\alpha})^{\frac{\beta}{\alpha+\beta}}$	/
⑦	$(\frac{e^{\beta} + 1}{e^{-\alpha x + \beta} + 1})^{\gamma}$	α, β, γ	Skewed S-shaped	/	$y = (e^{\beta} + 1)^{\gamma}$

Table S4. Parameter limits for each driver and functional form.

Functional form	Parameter	$(CO_2 - CO_{2_{2015}})/CO_{2_{2015}}$		$T^c_{gs} - T^c_{gs,pi}$		$(P^c_{gs} - P^c_{gs,pi})/P^c_{gs,pi}$	
		Lower limit	**Upper limit**	**Lower limit**	**Upper limit**	**Lower limit**	**Upper limit**
①	α	-1	1	-10	10	-1000	1000
②	α	-10	10	-10	10	-10	10
③	α	0	10	0	10	0	10
	β	-1	4	-30	30	-1	100
④	α	0	10	0	10	1	10
	β	0	10	0	10	0	10
⑤	α	0	100	0	100	0	100
	β	-10	10	-10	10	-10	10
⑥	α	0	100	0	100	0	100
	β	0	100	0	100	0	100
	γ	-10	10	-10	10	-10	10
⑦	α	0	100	0	100	0	100
	β	-10	10	-10	10	-10	10
	γ	0	10	0	10	0	10

Table S5. GGCM-irrigation-crop combinations of extreme-value yield responses with corresponding regional occurrences.

GGCM	Irrigation	Crop (Occurrence)
CYGMA1p74	*noirr*	*mai* (13), *ri1* (9), *ri2* (7), *soy* (8), *swh* (39)
ISAM	*firr*	*wwh* (4)
	noirr	*wwh* (1)
LDNDC	*noirr*	*mai* (10)
LPJmL	*firr*	*ri1* (3), *ri2* (1), *soy* (2)
	noirr	*mai* (3), *ri1* (16), *ri2* (17), *soy* (12), *swh* (7), *wwh* (5)
PEPIC	*noirr*	*mai* (1)
PROMET	*firr*	*wwh* (2)
	noirr	*mai* (7), *ri1* (10), *ri2* (9), *soy* (8), *swh* (2), *wwh* (4)
SIMPLACE-LINTUL5	*noirr*	*soy* (1)

Extreme-value yield occurrences are in parentheses.

Table S6. Functional forms and parameters for nitrogen responses.

Model	Functional form	Parameters
Michaelis-Menten	$\frac{\alpha x}{x+\beta}$	$\alpha,\ \beta$
Mitscherlich	$\alpha(e^{\beta x}-1)$	$\alpha,\ \beta$
George	$\alpha(0.99^{x}-1)+\ \beta x$	$\alpha,\ \beta$